Rigorous Modeling of the Kinetics of Calcium Carbonate Deposit Formation - CO_2 Effect

Raviv Segev, David Hasson, and Raphael Semiat
Rabin Desalination Laboratory, Grand Water Research Institute, Dept. of Chemical Engineering,
Technion-Israel Institute of Technology, Haifa 32000, Israel

DOI 10.1002/aic.12730
Published online August 5, 2011 in Wiley Online Library (wileyonlinelibrary.com).

Keywords: $CaCO_3$ precipitation, CO_2 hydration reaction, multicomponent ionic diffusion, simplified expressions

Introduction

The kinetics of $CaCO_3$ deposition on flow surfaces is of widespread interest in many engineering applications, notably cooling tower water systems and both thermal and membrane desalination processes. Comprehension of the kinetics of this system is closely allied to scale control efforts.

The complexity of the $CaCO_3$ precipitation system arises from the need to consider the combined role of several mass transfer, chemical reaction processes and flow effects. Kinetic models proposed in various studies are based on highly simplified assumptions.[1–14] We have recently derived a rigorous kinetic model which considered all processes involved in the precipitation system but included the simplification that the CO_2 hydration reaction was instantaneous.[15] This article completes our previous work by analyzing the effect of the CO_2 hydration reaction.

Precipitation mechanisms

The system considered is the same as that analyzed in our previous article and consists of wall deposition of a crystallizing $CaCO_3$ scale layer from a supersaturated solution in isothermal turbulent flow through a tube (Figure 1).

The overall reaction involved in the wall crystallization process of $CaCO_3$ is

$$\mathrm{Ca^{+2}} + 2\mathrm{HCO_3^-} \rightarrow \mathrm{CaCO_{3(s)}} + \mathrm{CO_2} + \mathrm{H_2O} \tag{1}$$

The main processes involved are the surface crystallization reaction

$$\mathrm{Ca^{+2}} + \mathrm{CO_3^{-2}} \rightarrow \mathrm{CaCO_{3(s)}} \tag{2}$$

which is followed by shifts of the ionic species participating in the process

$$\mathrm{H^+} + \mathrm{HCO_3^-} \Leftrightarrow \mathrm{CO_2} + \mathrm{H_2O} \tag{3}$$

$$\mathrm{HCO_3^-} \Leftrightarrow \mathrm{H^+} + \mathrm{CO_3^{-2}} \tag{4}$$

Correspondence concerning this article should be addressed to D. Hasson at hasson@tx.technion.ac.il.

CO_2 kinetics in carbonate systems

It is well established that the ionic species involved in the second dissociation constant of carbonic acid (H^+, HCO_3^-, and CO_3^{-2}) are at instantaneous equilibrium during the precipitation process. This is not the case for the first dissociation constant of carbonic acid since the reactant CO_2 is not in an ionic state.

The hydration and dehydration of CO_2 in carbonate solutions occur by the following parallel reaction mechanisms[16–18]

Acidic Mechanism:

$$CO_2 + H_2O \underset{k_{-1}}{\overset{k_1}{\longleftrightarrow}} H_2CO_3 \overset{\text{Instantaneous}}{\longleftrightarrow} HCO_3^- + H^+ \tag{5}$$

$$HCO_3^- \overset{\text{Instataneous}}{\longleftrightarrow} CO_3^{-2} + H^+ \tag{6}$$

$$\text{Alkaline Mechanism} \quad CO_2 + OH^- \underset{k_{-3}}{\overset{k_3}{\longleftrightarrow}} HCO_3^- \tag{7}$$

$$HCO_3^- + OH^- \overset{\text{Instantaneous}}{\longleftrightarrow} CO_3^{-2} + H_2O \tag{8}$$

Equations 5 and 7 describe finite rate reactions since the composition and decomposition of the CO_2 species occur through modification of the chemical structure of the CO_2 molecule. However Eqs. 6 and 8 describe instantaneous reactions since they involve only proton exchange.[19]

Table 1 summarizes correlations for the rate coefficients of reactions (5) and (7), while Table 2 lists the equilibrium constants of the instantaneous reactions (6) and (8).

Model Equations

The diffusional transport of the reacting species (H^+, OH^-, CO_3^{-2}, HCO_3^-, Ca^{+2}, CO_2) are given by

$$-\mathrm{D_i}\frac{\mathrm{d}^2 c_i}{\mathrm{dx}^2} = \mathrm{R_i} \tag{9}$$

where D_i is the diffusion coefficient of species i, and R_i is the reaction rate of the reacting species described by

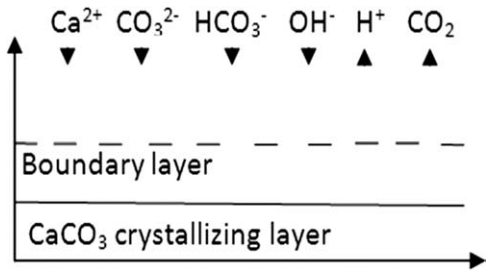

Figure 1. Transport of the reacting species from the solution bulk to the crystallizing layer.

Table 1. Rate Coefficents of the CO_2 Reactions

Reference	Rate Coefficient	Units	Reported Correlation
Pinsent et al.[20]	k_1	$\frac{1}{s}$	$\log k_1 = 329.85 - 110.541 \cdot \log T - \frac{17265.4}{T}$
Usdowski et al.[21]	k_{-1}	$\frac{1}{s}$	$\log k_{-1} = 13.558 - \frac{3617.1}{T}$
Pinsent et al.[20]	k_3	$\frac{l}{mol \cdot s}$	$\log k_3 = 13.635 - \frac{2895}{T}$
Usdowski et al.[21]	k_{-3}	$\frac{1}{s}$	$\log k_{-3} = 14.09 - \frac{5308.9}{T}$

$$R_{CO_2} = +k_1[CO_2] - k_{-1}[H_2CO_3^0] + k_3[CO_2] \cdot [OH^-] - k_{-3}[HCO_3^-] \quad (10)$$

$$R_{H^+} = +k_1[CO_2] - \frac{k_{-1}[H^+][HCO_3^-]}{K_5} - \frac{k_3[CO_2] \cdot K_w}{[H^+]} + k_{-3}[HCO_3^-] \quad (11)$$

$$R_{OH^-} = -k_3[CO_2][OH^-] + k_{-3}[HCO_3^-] + k_1[CO_2] - \frac{k_{-1}K_w[HCO_3^-]}{K_5[OH^-]} \quad (12)$$

$$R_{HCO_3^-} = +k_1[CO_2] - k_{-1}[H_2CO_3^0] + k_3[CO_2] \cdot [OH^-] - k_{-3}[HCO_3^-] \quad (13)$$

$$R_{CO_3^{-2}} = +k_1[CO_2] - \frac{k_{-1}[H^+]^2[CO_3^{-2}]}{K_5K_2} + k_3[CO_2] \cdot [OH^-] - \frac{k_{-3}[H^+][CO_3^{-2}]}{K_2} \quad (14)$$

$$R_{Ca^{+2}} = 0 \quad (15)$$

The species $H_2CO_3^0$ can be eliminated from Eqs. 10 and 13 using the equilibrium condition[17]

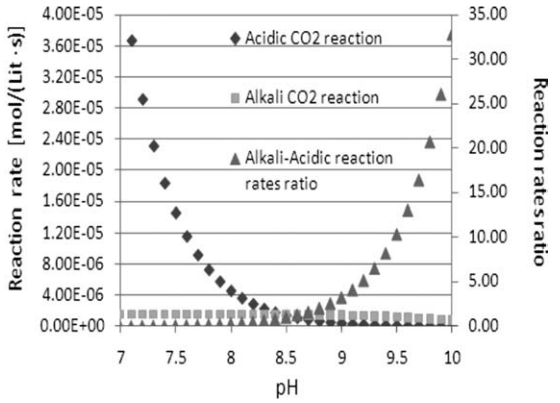

Figure 2. Acidic and alkaline CO_2 reaction rate and ratio of alkaline to acidity reaction rate as functions of the pH level (total alkalinity of 200 ppm as $CaCO_3$).

$$K_5 = [H^+][HCO_3^-]/[H_2CO_3^0] \quad (16)$$

As in our previous article, the surface integration step involved in $CaCO_3$ crystallization is described by the following rate expression[1–3]

$$J_{CaCO_3} = k_R[(Ca^{+2})_i(CO_3^{-2})_i - K'_{SP}] \quad (17)$$

where k_R ($m^4/s \cdot mol$) is assumed to depend on temperature according to the Arrhenius equation

$$\ln k_R = \ln A - E/RT \quad (18)$$

Comparison between CO_2 hydration reaction and CO_2 diffusion

Values of the acidic and alkaline reaction rates, respectively, were calculated using the rate coefficients listed in Table 1 and are displayed in Figure 2 as functions of the pH level at a total alkalinity of 200 ppm as $CaCO_3$. Figure 3 displays similar plots for a total alkalinity of 500 ppm.

It is seen that there is a pH range where the rate limiting step is the acidic reaction, a pH range where the rate limiting step is the alkali reaction, and there is a pH range where both reactions are important and cannot be neglected. The dominant mechanism may be assumed to be that where one of the reaction rates (acidic or alkaline) is at least five times higher than that of the alternative mechanism. Table 3 summarizes pH limits of the dominant reaction based on the aforementioned criterion.

Since the CO_2 concentration becomes vanishingly small at high pH levels, the dominant mechanism affecting the $CaCO_3$

Table 2. Equilibrium Constants of the Instantaneous Reactions

Reference	Equilibrium reaction	Equilibrium Constant	Reported Correlation
Plummer and Busenberg[22]	$\frac{[H^+][HCO_3^-]}{[CO_2]}$	K_1	$\log K_1 = -356.3094 - 0.06091964 \cdot T + \frac{21834.37}{T} + 126.8339 \cdot \log T - \frac{1684915}{T^2}$
Plummer and Busenberg[22]	$\frac{[H^+][CO_3^{-2}]}{[HCO_3^-]}$	K_2	$\log K_2 = -107.8871 - 0.0325849 \cdot T + \frac{5151.79}{T} + 38.92561 \cdot \log T - \frac{563713.9}{T^2}$
Harned and Hamer[23]	$[H^+][OH^-]$	K_w	$\log K_w = 22.801 - 0.010365 \cdot T - \frac{4787.3}{T} - 7.1321 \cdot \log T$

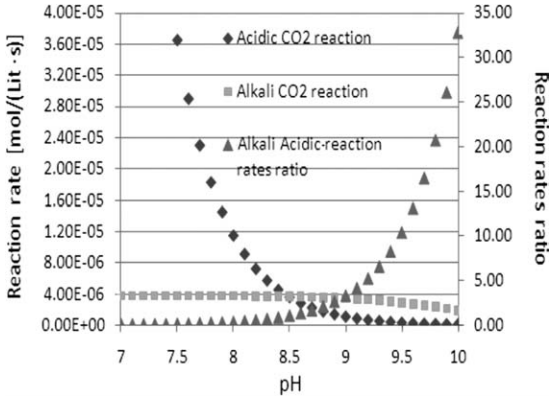

Figure 3. Acidic and alkaline CO_2 reaction rate and ratio of alkaline to acidity reaction rate as functions of the pH level (total alkalinity of 500 ppm as $CaCO_3$).

precipitation process is the acidic CO_2 hydration reaction. The relative extents of the CO_2 reaction and of the CO_2 diffusion may be evaluated by comparing the typical reaction time of the acidic reaction with the typical diffusion time of the CO_2 species. The typical reaction time is given by[25]

$$t_{Ac} = \left(k_1 + \frac{k_{-1}}{K_5}([H^+] + [HCO_3^-])\right)^{-1} \tag{19}$$

where k_1 and k_{-1} are the acidic forward and backward reaction constant, respectively and t_{Ac} the typical reaction time for alkali and acidic mechanisms, respectively.

The typical diffusion time is given by

$$t_D = \frac{D_{CO_2}}{k_{CO_2}^2} \tag{20}$$

where D_{CO_2} is the diffusion coefficient of the CO_2 species at 25°C and k_{CO_2} is the mass-transfer coefficient of the CO_2 species.

Table 4 displays the difference between the diffusion time and the acidic reaction time at various *Re* numbers and various total alkalinity levels. Since the CO_2 diffusion and the reaction occur simultaneously, the dominating effect is the process occurring more rapidly. It is seen that at the lowest *Re* number of 4,400 the reaction time of 2.75–6.43 msec is much more rapid than the diffusion time that requires 251 msec. This trend is reversed at high *Re* numbers. For $Re = 22{,}200$ the diffusion time of 1.71 ms is more rapid than the reaction time of 2.75–6.43 msec.

Influence of the CO_2 hydration reaction on the $CaCO_3$ precipitation rate

The influence of the CO_2 hydration reaction on the precipitation rate was analyzed by comparing results calculated assuming CO_2 equilibrium[15] with results taking into account the kinetics of the CO_2 reaction. Table 5 lists values of the parameters adopted in the simulation study. The range of chemical parameters analyzed was: total alkalinity of 100–500 [ppm as $CaCO_3$] and calcium of 100–400 [ppm]. The range of *Re* numbers was 4,400 to 22,200.

Figure 4 displays limiting pH levels at which the $CaCO_3$ precipitation rate based on CO_2 equilibrium deviates by less than 10% from results calculated in the presence of the CO_2 hydration reaction. The upper bound of each of the *Re* number bands represents absolute deviation levels corresponding to the high calcium and alkalinity concentrations and the lower bound, to the lower calcium and alkalinity concentrations. It is evident that high deviations occur only at the lowest *Re* numbers, while deviations are negligibly small at the highest *Re* number of 22,200.

Table 3. Extent of the Dominant Mechanism

pH level range	Dominant mechanism
7.0-8.0	Acidic
8.0-9.2	Acidic and Alkali
9.2-10.0	Alkali

Table 4. Reaction and Diffusion Time at Various Conditions

Total alkalinity [ppm]	Reaction time [msec]	Re 4400 Diffusion time [msec]	Re 11100 Diffusion time [msec]	Re 22200 Diffusion time [msec]
500	2.75	251	54.1	1.71
400	3.45			
300	6.43			
200	4.60			

Table 5. Parameters used in the Simulation Analyses

K_R	$3.68\cdot10^{-5}$ [m^4/(mol sec)]	D_H	$9.31\cdot10^{-9}$ [m^2/sec]
K_{sp}	$3.32\cdot10^{-3}$ [mol^2/m^6]	D_{OH}	$5.27\cdot10^{-9}$ [m^2/sec]
K_5	$1.71\cdot10^{-1}$ [mol/m^3]	D_{CO2}	$2.00\cdot10^{-9}$ [m^2/sec]
pH	7-11	D_{HCO3}	$1.13\cdot10^{-9}$ [m^2/sec]
U	24.25-198 [m/sec]	D_{CO3}	$0.97\cdot10^{-9}$ [m^2/sec]
Temp.	25 [°C]	D_{Ca}	$0.79\cdot10^{-9}$ [m^2/sec]

Concluding Remarks

The analyses described in this article and in our previous publication[15] enable prediction of the anticipated $CaCO_3$ precipitation rate in scale-prone systems, notably cooling water towers, thermal desalination units and membrane processes. The dominant mechanism under a wide range of conditions is convective mass transfer.

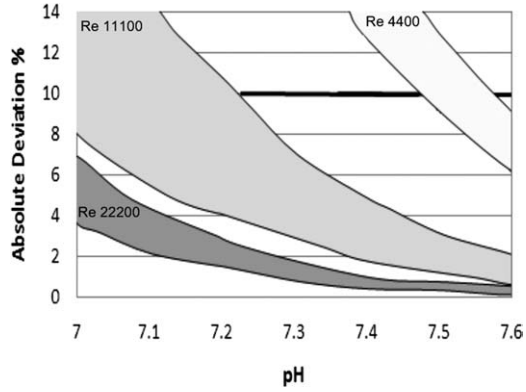

Figure 4. Absolute deviation ranges according to various total alkalinities, Ca^{+2} concentrations and *Re* numbers.

The analyses hold for systems free from impurities such as Fe^{2+}, Fe^{3+}, Zn^{2+} and Mg^{2+} which can alter significantly the surface precipitation reaction and enhance the role of the surface reaction mechanism.[24] Predictions based on analyses neglecting the effect of impurities provide an upper limit to the anticipated precipitation rate. Obviously, extension of available data on the effect of impurities on the surface reaction will widen the applicability of theoretical predictions of $CaCO_3$ scaling rates.

Literature Cited

1. Reddy MM, Nancollas GH. Crystallization of calcium carbonate. I: Isotopic exchange and kinetics. *J Colloid Interface Sci*. 1971;36:166–172.
2. Roques H, Girou A. Kinetic of the formation conditions of carbonate tartars. *Water Res*. 1974;8:907–920.
3. Wiechers HNS, Sturrock P, Marais GVR. Calcium carbonate crystallization kinetics. *Water Res*. 1975;9:835–845.
4. Dawe AR, Zhang Y, Kinetics of calcium carbonate scaling using observations from glass micromodels. *J Petrol Sci Eng*. 1997;18:179–187.
5. Zhang Y, Shaw H, Farquhar R, Dawe AR. The kinetics of carbonate scaling-application for the prediction of downhole carbonate scaling. *J Petrol Sci Eng*. 2001;29:85–95.
6. Paakkonen TM, Riihimaki M, Puhakka E, Muurinen E, Simonson CJ, Keiski RL. Crystallization fouling of $CaCO_3$- Effect of bulk precipitation on mass deposition on the heat transfer surface. In: Proceedings of International Conference on Heat Exchanger Fouling and Cleaning VIII. Saskatoon, SK, Canada; 2009:209–216.
7. Hasson D, Avriel M, Resnick W, Rozenman T, Windreich S, Mechanism of $CaCO_3$ scale deposition on heat-transfer surfaces. *Ind Eng Chem Fund*. 1968;7:59–65.
8. Hasson D, Sherman H, Biton M. Prediction of calcium carbonate scaling rates. *Proceedings of the International Symposium on Fresh Water From the Sea*. Las palmas, Spain: European Federation of Chemical Engineering; 1978;2:193–199.
9. Andritosos N, Kontopoulou M, Karabels AJ, Koutsoukos PG. Calcium carbonate deposit formation under isothermal conditions. *Can J Chem Eng*. 1996;74:911–919.
10. Turner CW, Smith DW. Calcium carbonate scaling kinetics determined from radiotracer experiments with calcium-47. *Ind Eng Chem Res*. 1998;37:439–448.
11. Khan SM, Budair MO, Zubair SM. A parametric study of $CaCO_3$ scaling in AISI 316 stainless steel tube. *Heat Mass Transfer*. 2001;38:115–121.
12. Chen T, Neville A, Mingdong Y. Influence of Mg^{2+} on $CaCO_3$ formation-bulk precipitation and surface deposition. *Chem Eng Sci*. 2006;61:5318–5327.
13. Quan Z, Chen Y, Ma C. Heat mass transfer model of fouling process of calcium carbonate on heat transfer surface. *Sci China Ser E Tech Sci*. 2008;51:882–889.
14. Koutsoukos PG. *Calcium carbonate scale control in industrial water systems*. In: Amjad Z, ed. *The Science and Technology of Industrial Water System*. Boca Raton, FL: CRC Press; 2010: 39–60.
15. Segev R, Hasson D, Semiat R. Rigorous modeling of the kinetics of calcium carbonate deposit formation. *AIChE J*. 2011;57: n/a. doi:10.1002/aic.12645
16. Kern DM, The hydration of carbon dioxide, *Journal of Chemical Education*, 1960:37, 14–22.
17. Astarita G. *Mass Transfer with Chemical Reaction*. Amsterdam: Elsevier; 1967.
18. Stumm W, Morgan JJ. *Aquatic Chemistry: Chemical Equilibria and Rates in Natural Waters*. 3rd ed. New York: John Wiley & Sons, Inc; 1996.
19. Astarita G, Savage DW, Bisio A. *Gas Treating with Chemical Solvents*. New York: John Wiley & Sons, Inc; 1983.
20. Pinsent BR, Pearson L, Roughton FJW, The kinetics of combination of carbon dioxide with hydroxide ions. *Trans Faraday Soc*. 1956;52:1512–1520.
21. Usdowski E. Reactions and equilibria in the systems CO_2- H_2O and $CaCO_3$-CO_2- H_2O (0–50 °c). *Neues Jb Miner Abh*. 1982;144:148–171.
22. Plummer LN, Busenberg E, The solubilities of calcite, aragonite and vaterite in CO_2 H_2O solutions between 0 and 90°C, and an evaluation of the aqueous model for the system $CaCO_3$-CO_2-H_2O. *Geochim Cosmochim Acta*. 1982;46:1011–1040.
23. Harned HS, Hamer WJ. The ionization constant of water. *J Am Chem Soc*. 1933;55:693–695.
24. Hasson D, Semiat R, Levicki M, Damiano D, Sher A. Inhibition of $CaCO_3$ scale deposition by trace concentration of some common ions. Proceedings of AWWA Water Quality Conference; November 14–18, 2004; San Antonio: Texas; 2004:19.
25. Zeebe RE, Wolf-Gladrow DA, Jansen H. On the time required to establish chemical and isotopic equilibrium in the carbon dioxide system in seawater. *Marine Chem*. 1999;65:135–153.

Manuscript received May 2, 2011, and revision received Jun. 22, 2011.